Incipient grain transport and pattern formation at a sand surface sheared by a continuous laminar flow. Part II: Large bed slope. Avalanche dominated regimes.

D. Doppler [*(1)], T. Loiseleux[(1,2)], P. Gondret[(1)] and M. Rabaud[(1)]

(1) Laboratoire Fluides, Automatique et Systèmes Thermiques (FAST) – Orsay – France
(2) Unité de Mécanique – Ecole Nationale Supérieure de Techniques Avancées (ENSTA)– Paris – France

Abstract

A linear narrow duct is used to explore the macroscopic effects of fluid-grains interactions on granular slopes. In this part II we show that the angle of avalanche evolves when a flow is present in the cell. This dependency is found to be linear for various glass beads diameter and is well fitted by a simple model including the Darcy pressure drop in the porous layer. For large enough values of the Shields number and of the tilt angle, the competition between avalanche and uphill erosion gives birth to exponentially growing vortex ripples. They rapidly saturate and propagate in the stream direction. Temporal growth rate is quite sensitive to tilt angle and bead diameter, but weakly to flow rate. In the saturated regime, mean amplitude is clearly correlated to the mean wavelength independently of control parameters, when the phase velocity depends mostly on tilt angle.

1. Introduction

The understanding of natural processes such as wind or water erosion is of main importance, as grain transport may have deep implication on climate, landscape and human activities. However, the existing models still fail to predict and control the macroscopic effects of the interactions between fluid and grains. One of those spectacular effects is the displacement of big amounts of sand by turbidity currents or by submarine avalanches; another is the ripples one can observe on the slopes of submarine dunes or on riverbeds. Even if the stability of a dry granular pile and the existence of a maximum stability angle above which dry granular matter flows have been widely explored, (Bagnold, 1954), few experiments have been performed in liquids (Courrech *et al.*, 2003a). Furthermore, to our knowledge, avalanche onset for a granular slope sheared by a hydrodynamic flow has never been studied. Several papers focus on the effect of a bed slope on the threshold of grain motion, showing that the tangential gravity component can, depending on its direction, strongly increase or decrease this threshold (Allen, 1982, Dyer, 1986, Fredsoe and Deigaard, 1992, Whitehouse and Hardisty, 1988), but these studies are restricted to small bed slopes and thus correspond to part I of this work.

We propose here an experiment where a tilted granular bed is sheared by a laminar continuous flow of water in a well-controlled linear geometry. Of course this configuration is much more simple than real hydrological systems in which flow is generally turbulent and geometry is complex, but we expect a better understanding of the effect of each basic parameter on the stability of granular slopes sheared by a hydrodynamic flow.

When the cell is inclined at large angle, and for current intensity larger than a threshold value, vortex-like sand ripples appear everywhere in the cell. These structures appear more similar to those observed during sedimentation in inclined channels, at the interface between clear fluid and suspended layer (Herbolzheimer, 1983) than to sand ripples encountered for small bed slopes (Bagnold, 1946, Allen, 1980, Coleman and Buckhard, 2000). Several theoretical models based on linear stability and viscous resuspension hypothesis have been developed for small slopes (Schaflinger *et al.*, 1995, Charru and Mouilleron-Arnould, 2002, Valance and Langlois, 2003) but they still fail in predicting initial wavelength. Model of the instability occurring at large angles is missing.

* Corresponding author: doppler@fast.u-psud.fr

2. Experimental set up

The experimental set-up consists of a very narrow linear flume (Fig.1), half-filled with well-sieved spherical glass beads of mean diameter d (±10 %), chosen in the range [90 µm, 220 µm]. Water flows from left to right by the means of a centrifugal pump, and imposes a constant shear stress on the bed all along the cell. This continuous hydrodynamic flow is considered to remain laminar for the velocity range used in our experiments.

The cell can rotate around its transversal axis up to 60°, downstream or upstream. The tilt angle b is defined as positive when the water flows uphill and as negative when it flows downhill. More details about the experimental set-up can be found in Part I.

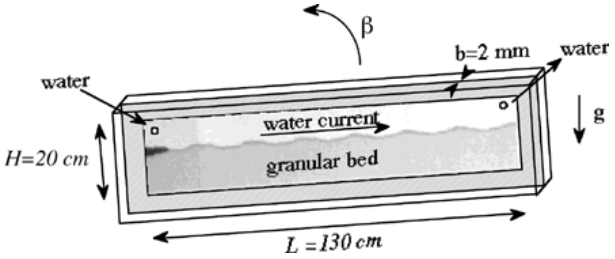

Fig. 1 – Scheme of the Hele-Shaw flume

Flat bed is first prepared by alternatively tilting the cell at large positive and negative angles. Each experiment is filmed with two synchronised CCD cameras fixed to the cell, so we can visualise half the length of the cell. A particle image velocimetry (PIV) software is used to determine the grain velocity.

The two independent control parameters are the flow rate Q and the tilt angle b.

In the following, we will use Shields number q calculated for a horizontal bed (cf. Part I) rather than Q to characterise the shear imposed by the flow:

$$q = 3.26 \frac{h Q h_w}{\Delta r \, g \, d \, b^2} \, , \qquad (1)$$

where h is the dynamic viscosity and Dr is the difference between grain and fluid densities.

3. Onset of avalanche

3.1 Experimental results

For $Q = 0$, we prepare a horizontal flat bed and we slowly tilt the cell until avalanche occurs, *i.e.* until a layer 3 to 5 grains thick starts to move downhill as a block. The mean avalanche angle obtained is $b_0 = 30.3 \pm 0.2°$ for $d = 130$ µm, which is similar to natural angles usually mentioned in the literature. This angle slightly increases with the grain diameter, possibly due to arching effects between the lateral walls (Courrech *et al.*, 2003b). If we repeat the same experiment with a constant uphill (respectively downhill) flow rate Q ? 0, the maximum stability angle is found to be larger (resp. smaller). Experimental results are reported on Fig. 2a for various particle diameters. For a given d, avalanche angle varies almost linearly with the Shields number, even if the slope seems slightly different for positive and negative b.

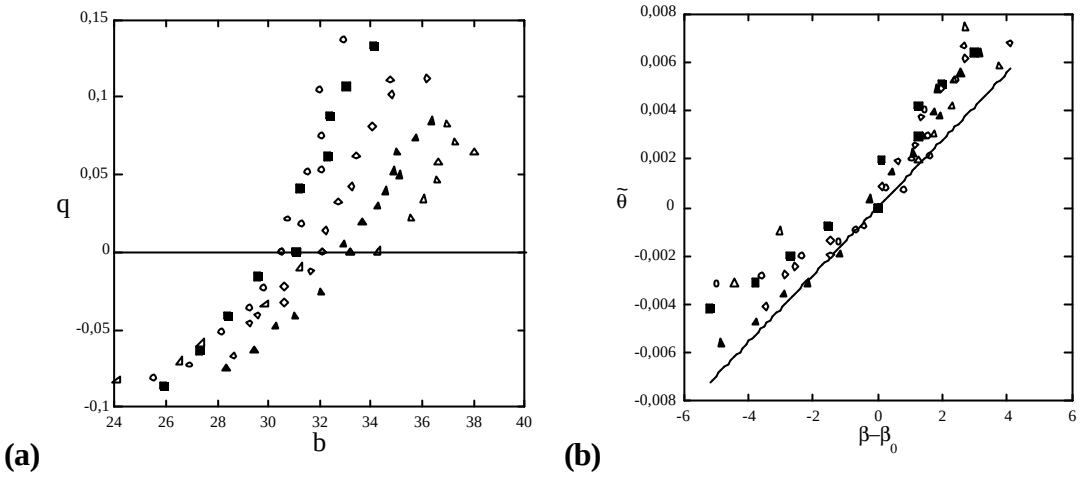

Fig. 2 – a) Maximum stability angle b as a function of the Shields number q for various grain diameter b) Variation of the maximum stability angle b-b_0 as a function of the modified Shields number q together with Eq. 2 . (—) (○) d = 90 µm, (■)d = 110 µm, (◇)d = 140 µm, (▲) d = 180 µm, (△) d = 220 µm

3.2 Two phases model

Conversely to the erosion model developed in Part I, we will now consider the granular matter as a continuous porous media. Indeed avalanche is a collective phenomenon, whereas erosion concerns individual particles. So let us consider a thin porous layer of height h, width b, length L and packing fraction c. Four forces are acting in the direction of the flow: the projection of the apparent weight of the grains F_W, a friction force F_f between the layer and the bulk, a force $F_t = tbL$ with $t \approx 3.26\,h\overline{U}/b$ due to the flow shearing the upper surface of the layer and an internal force $F_h = -\Delta P bh$ calculated applying Darcy's law $\Delta P/L = -12\,h\overline{U}/b^2$. Just before the layer starts sliding, equilibrium writes:

$$-F_W \sin b = F_f + F_t + F_h.$$

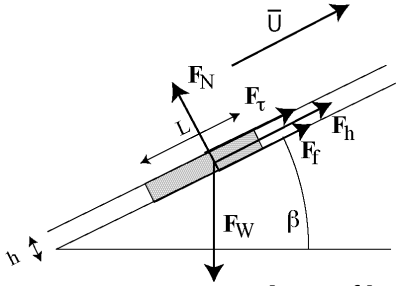

Fig. 3 – Sketch of the forces acting on a porous layer of height h and compactness c

This gives for the modified Shields number $\tilde{q} = q\dfrac{d}{b}\cos b_0$:

$$\tilde{q} = c\frac{h}{b}\left(1 + 3.68\frac{h}{b}\right)^{-1}\sin\left(b - b_0\right). \qquad (2)$$

For small values of, our model predicts a quasi-linear evolution of avalanche angle with mean flow rate. Moreover, with a common value of packing fraction c = 0.56, this model fits quite well the data obtained for various diameters in both directions (Fig. 2.b) and gives h ~ 0.5 mm. This value is comparable with the

typical thickness of the avalanches we observed in our experiments, and gives an internal force F_h of the same order as the shear force F_t.

3. Vortex ripples

3.1 Qualitative description

As shown in Part I for small tilt angles, the bed remains flat, solid-like, for low values of Shields number, while grains start rolling and triangular ripples appear everywhere in the cell for larger q (Fig. 4).

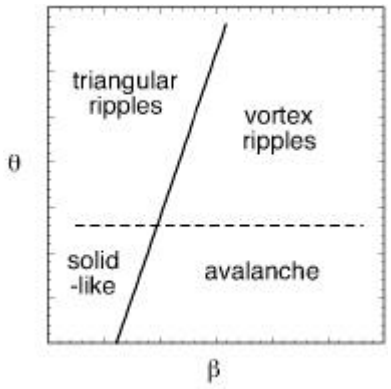

Fig. 4 – Sketch of different states of the granular bed for water flowing uphill
(____ onset of avalanche, _____ onset of erosion)

For large tilt angles, avalanches are observed for small uphill flow rates, but periodically spaced ripples are observed for strong uphill current (Fig. 4). These structures appear simultaneously all along the duct due to the strong but spatially constant shear between the avalanching grain layer and the water flowing in the opposite direction.

Figure 5 shows that these structures are quite different from the triangular ripples observed in the case of lower tilt angles (Fig. 6 of Part I) for which no avalanche exists. As can be seen on Fig. 5.b, a strong vortex separates two successive ripples, and for that reason we will call them vortex ripples.

On Fig. 5a one can see that the fluid drags grains up to the crest (from C'' to A and from C to A'). Particles take off and land in the trough (between A and C). Some of the grains impact the next ripple in C, triggering an avalanche of the surface layer that would stop near the crest of the first ripple in B (here to the left from C to B). Even if the global particle transport rate can be negative, the vortex ripples propagate in the stream direction (to the right in Fig. 5).

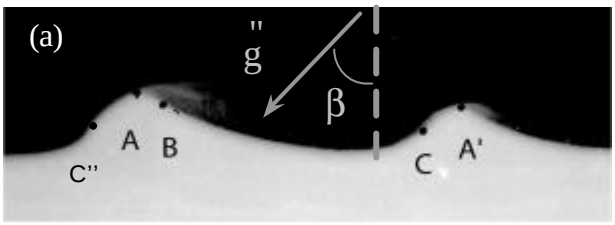

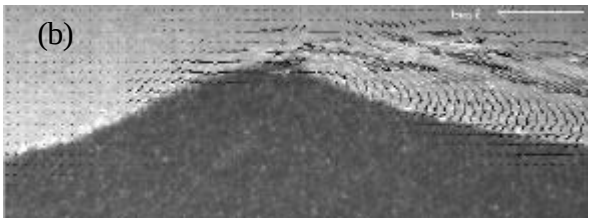

Fig. 5 – a) Image of two developed vortex ripples (note the direction of gravity **g** indicated by the arrow)
b) The existence of a vortex between two ripples is evidenced performing Particle Image Velocimetry for grains

In the following we will present results for parameter values far from the onset values materialised by the borderlines of Fig. 4. Indeed the transition between two types of structures is not well defined, as hybrid

behaviour is observed. It is worth noticing that when water and grains flow in the same direction (*i.e.* $b < 0$), no structures are observed.

3.2 Global behaviour

Each experiment is filmed and each image is processed to extract the height of the interface $h(x,t)$. This height is coded in grey levels (the higher the lighter) and displayed as horizontal lines on a spatiotemporal diagram (Fig. 6). The stripes correspond to the trajectories of ripples: they propagate with a constant speed.

At short times, ripples appear everywhere in the cell with an initial wavelength $\lambda \sim 12$ mm and their amplitude grow rapidly, following an exponential law (Fig.7.a). After several doublings of wavelength, the structures saturate due to nonlinearities and may be characterised by a unique amplitude A_{sat}, wavelength l_{sat} and phase velocity c. Contrary to the case of triangular waves described in Part I, this behaviour is consistent with a linear stability model for two fluids flowing in opposite directions.

At long times, structures saturate everywhere in the cell except near the inlet, where small propagating ripples are always present. On Fig. 6, the bottom picture shows the typical aspect of the interface for a given time in this regime. When moving away from the input (increasing x), the structures exhibit a spatial exponential growth of its amplitude, several period doublings and then saturation.

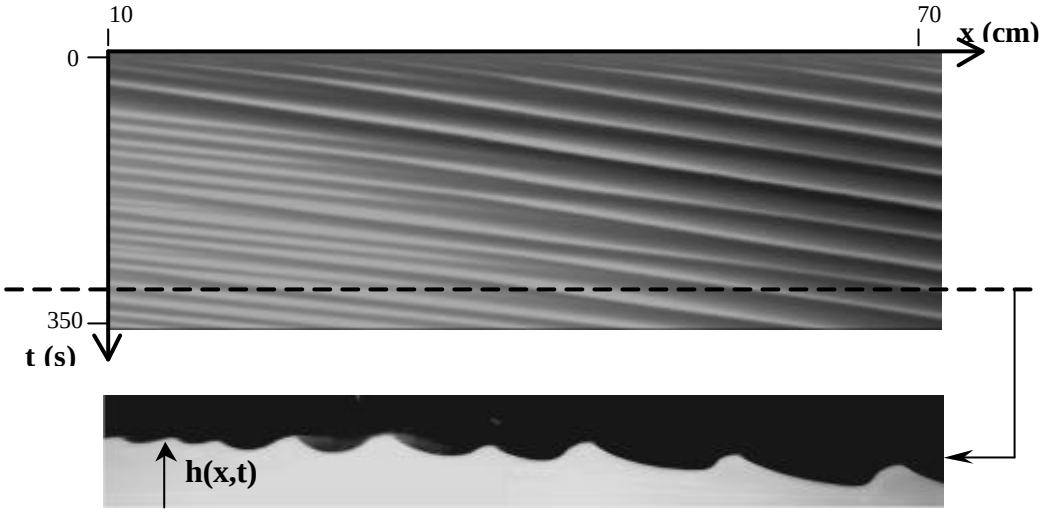

Fig. 6 – Spatiotemporal diagram: $h(x,t)$ is coded in a grey scale (d = 112 μm, $b = 38°$, $q = 0.3$) The bottom picture shows the typical aspect of the interface for long times (t ˜ 300 s). Global grain transport is negative, grains accumulated upstream (small x) and the mean interface is not parallel anymore to the cell axis.

3.3 Growth rates

From spatiotemporal data we are able to follow each ripple. The time evolution of the amplitude A of one ripple is plotted on Fig. 7.a in semi-logarithmic scales. At short times, the growth is exponential and the slope of the linear part of the curve gives the temporal growth rate σ. Mean values of σ measured for several experiments are displayed on Fig. 7.b. Data show a weak dependence on Shields number but a strong influence of tilt angle and diameter on temporal growth rate σ.

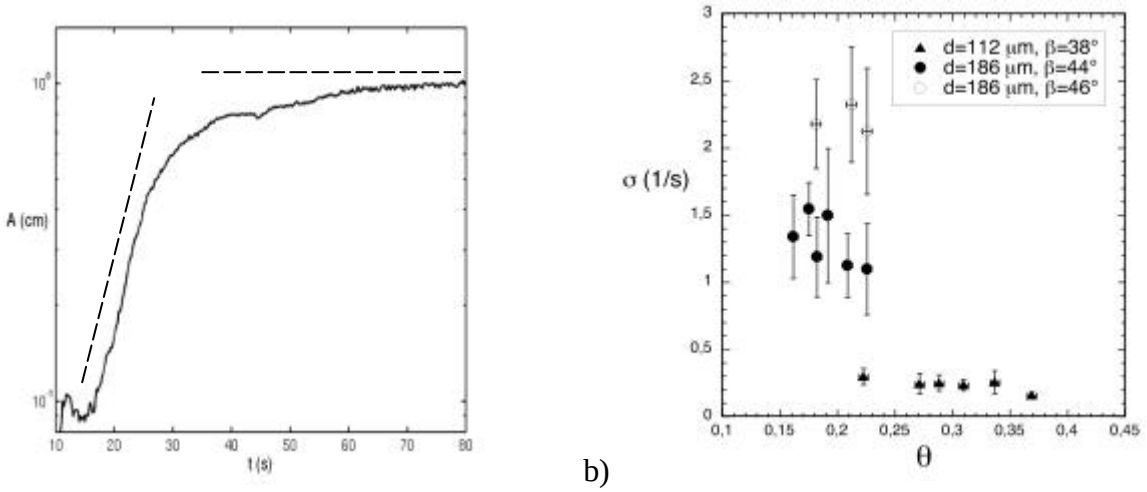

a) b)

Fig. 7– a) Time evolution of the amplitude A of a ripple in semi logarithmic scale.
Dashed lines enhance the exponential growth, which is followed by a saturation stage.
b) Temporal growth rate σ as a function of Shields number *q*
(σ) *d*=112µm, *b*=38°, (λ) *d*=186µm, *b*=44°, ( ) *d*=186µm, *b*=46°

3.3 Saturated state

As previously stated, saturated structures may be characterised by a unique amplitude A_{sat}, wavelength l_{sat} and phase velocity c for a given value of parameters *q*, *b* and *d*. We measured mean values of A_{sat}, l_{sat} and *c* far enough from the input and long enough after the beginning of the experiment to be sure to visualize saturated structures. Phase velocity exhibits a weak dependence on the flow rate and on the tilt angle, but is strongly influenced by the grain diameter. The mean amplitude of the saturated waves seems to be correlated to the mean wavelength for various values of *q*, *b* and *d*.

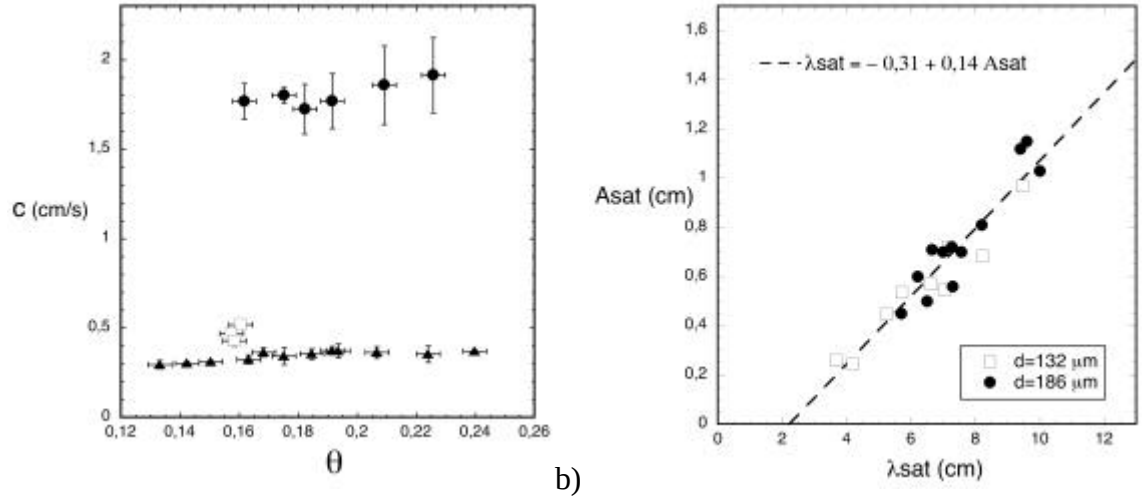

a) b)

Fig. 8 – a) Mean phase velocity *c* of the saturated ripples function of Shields number *q*
(σ) *d*=112µm, *b* = 38°, (≤) *d*=132µm, *b* = 40°, (λ) *d*=186µm, *b* = 44°
b) Mean amplitude of the saturated ripples A_{sat} function of mean wavelength l_{sat}, for various *b* and *q*

4. Conclusion

We studied the effect of water flow rate on maximum stability angle of a grain slope. We showed a linear dependency of avalanche angle on Shields number, which can be explained qualitatively and quantitatively with a simple model involving a Darcy force due to the water flowing through the porous medium.
Above avalanche angle, we exhibited the existence of vortex-like ripples for strong enough uphill water flow. These ripples always propagate in the stream direction by the way of erosion and deposition mechanisms. In early stages, ripples appear homogeneously everywhere in the cell and grow exponentially. The temporal growth rate is weakly influenced by the flow rate but depends on tilt angle and grain diameter. At later times, structures saturate. The saturated state is characterised by a constant phase velocity, a constant wavelength and a constant amplitude almost everywhere in the cell except near the entrance where fetch effect is observed as for the sea-wave formation. When varying the particle diameter, flow rate and tilt angle, we exhibited a correlation between amplitude and wavelength independently on the parameters. Phase velocity seems to be influenced mostly by grain diameter.

Acknowledgment

The authors are grateful to Olivier Chaplain for his help during experiments.
This work is supported by the French Ministry of Research. Actions Concertées Incitatives Jeunes Chercheurs n°2134 *Dynamique d'interfaces sable/fluide : Application à la morphologie des fonds marins.*

References

J. R. L. Allen, Sand waves: a model of origin and internal structures, *Sediment. Geol.*, Vol. 26, pp. 281-328, 1980.
J. R. L. Allen, Simple models for the shape and symmetry of tidal sand waves 1, 2 et 3, *Marine geology*, Vol. 48, pp. 31-49, 1982.
R.A. Bagnold, Motion of waves in shallow water. Interaction of waves and sand bottom, *Proc. Roy. Soc., London*, Ser. A , Vol.187, 1946.
R.A. Bagnold, Experiments on a gravity-free dispersion of large solid spheres in Newtonian fluid under shear, *Proc. Roy. Soc., London*, Ser. A, Vol. 225, 1954
F. Charru and H. Mouilleron-Arnould, Instability of a bed of particles sheared by a viscous flow, *J. Fluid Mech.*, Vol. 452, pp. 303-323 , 2002.
Coleman, S. and Burkhard, E. Sand wavelets in laminar open-channel flows, *J. of Hydr. Res.* , Vol. 38, Nº5, 2000.
S. Courrech du Pont, P. Gondret, B. Perrin and M. Rabaud, Granular avalanches in Fluids, *Phys. Rev. Lett.*, Vol. 90, 044301, 2003a.
S. Courrech du Pont, P. Gondret, B. Perrin and M. Rabaud, Wall effects on granular heap stability, *Europhys. Lett.*, Vol. 61, pp. 492-498, 2003b.
Damgaard J.S., Whitehouse R.J.S., and Soulsby R.L. Bed-load sediment transport on steep longitudinal slopes, *J.Hydraulic Eng.*, ASCE 123, No.12, pp. 1130-1138, 1997.
K. R. Dyer, 1986, Costal and estuarine sediment dynamics, *Wiley*.
Fredsoe, J, and Deigaard R., Mechanics of coastal sediment transport, *World Scientific. Advanced series on ocean engineering*, Vol. 3. ,1992
E. Herbolzheimer, Stability of the flow during sedimentation in inclined channels, *Phys. Fluids*, Vol. 26, pp. 2043-2054, 1983.
U. Schaflinger, A. Acrivos, H. Stibi, An experimental study of viscous resuspension in a pressure-driven plane channel flow, *International Journal of Multiphase Flow*, Vol. 21, pp. 693-704, 1995.

A. Valance and V. Langlois, Formation of Ripples over a sand bed. Part I: Laminar boundary flow, preprint. 2003.
R.J.S. Whitehouse and J. Hardisty, Experimental assessment of two theories for the effect of bedslope on the threshold of bedload transport. *Marine Geology*, Vol. 79, pp.135-139, 1988.